

METABOLISM

Pyrimidines maintain mitochondrial pyruvate oxidation to support de novo lipogenesis

Umakant Sahu^{1,2,†}, Elodie Villa^{1,2,†}, Colleen R. Reczek^{2,3}, Zibo Zhao^{1,2}, Brendan P. O'Hara^{1,2}, Michael D. Torno^{1,2}, Rohan Mishra⁴, William D. Shannon⁴, John M. Asara⁵, Peng Gao⁶, Ali Shilatifard^{1,2}, Navdeep S. Chandel^{1,2,3}, Issam Ben-Sahra^{1,2,*}

Cellular purines, particularly adenosine 5'-triphosphate (ATP), fuel many metabolic reactions, but less is known about the direct effects of pyrimidines on cellular metabolism. We found that pyrimidines, but not purines, maintain pyruvate oxidation and the tricarboxylic citric acid (TCA) cycle by regulating pyruvate dehydrogenase (PDH) activity. PDH activity requires sufficient substrates and cofactors, including thiamine pyrophosphate (TPP). Depletion of cellular pyrimidines decreased TPP synthesis, a reaction carried out by TPP kinase 1 (TPK1), which reportedly uses ATP to phosphorylate thiamine (vitamin B1). We found that uridine 5'-triphosphate (UTP) acts as the preferred substrate for TPK1, enabling cellular TPP synthesis, PDH activity, TCA-cycle activity, lipogenesis, and adipocyte differentiation. Thus, UTP is required for vitamin B1 utilization to maintain pyruvate oxidation and lipogenesis.

Pyrimidine nucleotides are necessary for nucleic acid synthesis, glycosylation, phospholipid synthesis, cellular biomass, and homeostasis (1–4). Pyrimidine production occurs through two metabolic pathways: the de novo pyrimidine synthesis pathway and the salvage pathway. The former results from the assembly of the pyrimidine ring from amino acids and other small molecules, whereas the latter requires recycling of pyrimidine nucleosides, such as uridine, from the surrounding environment. These pathways are distinct and separate processes (1, 5). Three metabolic enzymes produce uridine monophosphate (UMP) from de novo pyrimidine synthesis.

The rate-limiting step of the de novo pyrimidine pathway is dihydroorotate synthesis from glutamine, aspartate, bicarbonate, and adenosine 5'-triphosphate (ATP) by the cytosolic tri-catalytic enzyme CAD (carbamoyl-phosphate synthetase 2, aspartate transcarbamoylase, and dihydroorotate) (6, 7). Dihydroorotate dehydrogenase (DHODH) oxidizes dihydroorotate in the mitochondria to produce orotate, which UMP synthase (UMPS) converts to UMP in the cytosol (8–10). Cytidine triphosphate (CTP) synthase (CTPS) converts UTP to CTP after UMP phosphorylation.

UTP and CTP serve as building blocks for nucleic acid synthesis (11, 12) (Fig. 1A). But UTP

also supports glycosylation processes (13, 14), and CTP functions in phospholipid synthesis (15, 16) (Fig. 1A). Although purines, such as adenylates (ADP, ATP), participate in energy metabolism, including glycolysis and the tricarboxylic citric acid (TCA) cycle (17, 18), direct effects of pyrimidines on central carbon metabolism activity have not been described.

Requirement of cellular pyrimidines for pyruvate catabolism

To understand how pyrimidine nucleotides affect cellular metabolism, we performed targeted metabolite profiling of human cervical cancer cells (HeLa) treated with either solvent or the DHODH inhibitor brequinar (BRQ) at several time points (table S1). BRQ treatment rapidly decreased abundance of pyrimidine intermediates. Within 4 hours, citrate concentration decreased, whereas pyruvate concentrations increased (Fig. 1, B and C). By contrast, the DHFR inhibitor methotrexate (MTX), which affects one-carbon metabolism and purine and thymidylate production, had no effect on steady-state pyruvate and citrate levels (Fig. 1D). To study pyrimidine depletion independent of mitochondrial DHODH (19), we used CRISPR-Cas9 to generate cells lacking CAD (Δ CAD) or UMPS (Δ UMPS) human embryonic kidney 293E (HEK293E) and HeLa cell lines, respectively (fig. S1, A and B), which showed a decrease in de novo pyrimidine synthesis, as indicated by reduced 14 C incorporation from aspartate into RNA (fig. S1C). Uridine depletion in Δ CAD or Δ UMPS cells reduced cell proliferation and resulted in uridine auxotrophy (fig. S1, D and E). Depleting the de novo purine enzyme phosphoribosylglycinamide formyltransferase (GART) (Δ GART) (20) in HEK293E cells inhibited de novo purine synthesis and induced purine auxotrophy (fig. S1, F to H). Similarly to DHODH inhibition, lack of uridine in Δ UMPS HEK293E cells depleted cellular py-

rimidines, resulting in decreased abundance of citrate and increased amounts of pyruvate (Fig. 1E and fig. S1I). Subjecting cells to 16 hours of pyrimidine depletion did not exert a widespread impact on other metabolic pathways (fig. S2A and table S2). Furthermore, this period of pyrimidine deprivation did not trigger any changes in the abundance of pyrimidine enzymes or in the activity of the mechanistic target of rapamycin complex 1 (mTORC1), a critical regulator of cellular metabolism (21, 22) (fig. S2, B and C).

To assess whether changes in abundance of pyruvate and citrate were associated with alterations in glycolysis and the TCA cycle, we used stable isotope tracing of [13 C₆]-glucose or [13 C₃]-pyruvate in control cells or cells deprived of pyrimidines (Fig. 1F and fig. S3A). The citrate (M+2)/pyruvate (M+3) enrichment ratio decreased upon pyrimidine depletion, whereas glucose entry remained unchanged (Fig. 1, G and H, and fig. S3, B and C). Pyrimidine depletion also decreased abundance of other TCA-cycle metabolites such as α -ketoglutarate (M+2), succinate (M+2), and fumarate (M+2) in Δ CAD and Δ UMPS HEK293E cells (fig. S3C), without noticeable changes in amounts of glycolytic intermediates (fig. S3, D through F). By contrast, purine deprivation in Δ GART cells decreased the abundance of glycolytic intermediates (fig. S3G). Inhibition of de novo pyrimidine synthesis with BRQ and the UMPS inhibitor pyrazofurin (PRZ)—or genetic deletion of CAD—consistently decreased pyruvate catabolism and TCA-cycle activity in various human cancer cell lines and mouse embryonic stem (mES) cells (Fig. 1, I and J, and fig. S4, A to E). However, depletion of purines did not affect this process (fig. S4, F and G). To determine if the regulation of pyruvate catabolism by pyrimidines is conserved across species, we used *Saccharomyces cerevisiae* (yeast) and *Mus musculus* (mouse) as model systems. Ura3-deficient (*ura3*) *S. cerevisiae* cells, which are uracil auxotrophs (fig. S4H), exhibited decreased pyruvate catabolism upon acute (15-min) uracil depletion (Fig. 1K and fig. S4, I and J). Mice treated with a DHODH inhibitor also showed lower liver pyruvate catabolism than did vehicle-treated mice (Fig. 1, L and M). These findings demonstrate that pyrimidine abundance can influence pyruvate catabolism from unicellular yeast to mouse and human cells.

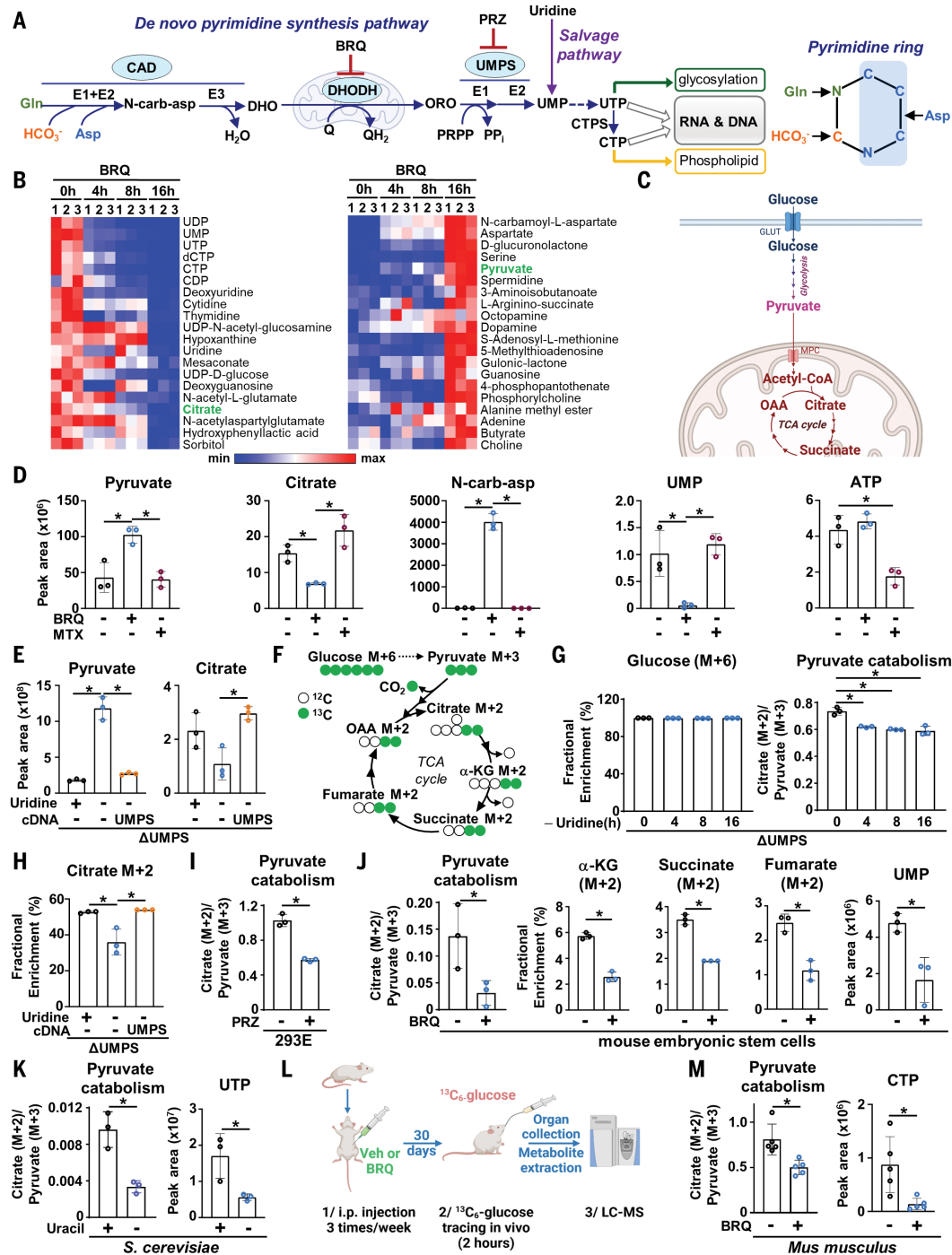
Cellular pyrimidines support pyruvate dehydrogenase activity

The mitochondrial pyruvate dehydrogenase (PDH) complex decarboxylates pyruvate into acetyl-coenzyme A (acetyl-CoA), which enters the TCA cycle. We assessed PDH activity by measuring the release of [14 C]-CO₂ resulting from the oxidation of [1- 14 C]-pyruvate (Fig. 2A). Depletion of uridine in Δ UMPS or Δ CAD cells decreased cellular PDH activity, which was

¹Department of Biochemistry and Molecular Genetics, Feinberg School of Medicine, Northwestern University, Chicago, IL 60611, USA. ²Robert H. Lurie Comprehensive Cancer Center, Northwestern University, Chicago, IL 60611, USA. ³Department of Medicine, Northwestern University Feinberg School of Medicine, Chicago, IL 60611, USA.

⁴BioRankings, St. Louis, MO 63108, USA. ⁵Mass Spectrometry Core, Beth Israel Deaconess Medical Center, Department of Medicine, Harvard Medical School, Boston, MA 02115, USA.

⁶Metabolomics Core Facility, Robert H. Lurie Comprehensive Cancer Center, Northwestern University, Chicago, IL 60611, USA. *Corresponding author. Email: issam.ben-sahra@northwestern.edu
†These authors contributed equally to this work.

**Fig. 1. Depletion of cellular pyrimidines inhibits pyruvate catabolism.**

(A) Illustration and metabolic role of the de novo pyrimidine synthesis pathway. The DHODH inhibitor brequinar (BRQ) and UMPS inhibitor pyrazofurin (PRZ) are indicated. (B) Steady-state metabolite profiles measured by liquid chromatography–tandem mass spectrometry (LC-MS/MS) of HeLa cells treated with BRQ (1 μ M). (C) Glucose fate through glycolysis and TCA cycle. (D) Steady-state levels of pyruvate, citrate, *N*-carbamoyl-L-aspartate, UMP, and ATP measured by LC-MS/MS in HeLa cells treated with vehicle (DMSO, dimethyl sulfoxide), BRQ (1 μ M), or methotrexate (MTX, 4 μ M) for 16 hours. (E) Same as shown in (D), but in Δ UMPS HEK293E cells reconstituted or not with UMPS cDNA. (F) Carbon flow schematic from $^{13}\text{C}_6$ -glucose into the TCA cycle. (G) Fractional enrichment (%) of ^{13}C -labeled glucose ($M+6$) from $^{13}\text{C}_6$ -glucose labeling in Δ UMPS HEK293E cells exposed to uridine withdrawal time course. (H) Fractional enrichment (%) of citrate ($M+2$) from $^{13}\text{C}_6$ -glucose labeling in mouse embryonic stem cells.

(I) Pyruvate catabolism from HEK293E cells labeled with $^{13}\text{C}_3$ -pyruvate and treated with vehicle (DMSO) or PRZ (1 μ M) for 16 hours. (J) Pyruvate catabolism and fractional enrichment (%) of ^{13}C -labeled metabolites derived from $^{13}\text{C}_3$ -pyruvate in mouse embryonic stem cells treated as in (I). (K) Pyruvate catabolism measured in *S. cerevisiae* *ura3 Δ* cells labeled with $^{13}\text{C}_3$ -pyruvate for 30 min. (L) Experimental design of the $^{13}\text{C}_6$ -glucose isotope tracing in mice. (M) Measurement of pyruvate catabolism in livers of mice treated with vehicle (PBS 70%, PEG-400 30%) or BRQ (20 mg/kg). Data in (M) are mean \pm SD. n = 5 mice. For all the other panels, data are mean \pm SD. n = 3 independent replicates. *P < 0.05 for multiple comparisons calculated using one-way analysis of variance (ANOVA) with Tukey's honest significant difference (HSD) test [(D), (E), (G), and (H)] or using a two-tailed Student's t test for pairwise comparisons [(I), (J), (K), and (M)].

rescued by adding back uridine or reexpressing UMPS in Δ UMPS cells (Fig. 2, B and C, and fig. S5A). The pyrimidine-dependent decrease in PDH activity appeared not to result from changes in abundance or protein products of the genes that function in pyruvate metabolism or glycolysis (Fig. 2D and fig. S5B). Uridine-starved Δ CAD HEK293E cells showed decreased acetyl-CoA (M+2) derived from pyruvate (M+3) (Fig. 2E). Similarly, acetyl-CoA production was diminished in HeLa cells treated with BRQ (fig. S5C) and in Δ CAD A375, Δ CAD A549, and Δ CAD CAL-51 cancer cells depleted of uridine (fig. S5D).

Because PDH and the TCA cycle generate the reducing equivalent nicotinamide adenine dinucleotide (NADH) in the mitochondria, we investigated whether pyrimidine depletion altered abundance of mitochondrial NAD(H). DHODH inhibition decreased amounts of mitochondrial NADH but not those of NAD⁺ in HeLa cells (Fig. 2, F and G). Similarly, genetic deletion of UMPS or CAD decreased mitochondrial NADH, but not NAD⁺, in the absence of exogenous uridine (Fig. 2, H and I, and fig. S5E). In various Δ CAD cancer cell lines, elimination of uridine lowered the mitochondrial NADH/NAD⁺ ratio (Fig. 2J and fig. S5, F to H).

Because NADH serves as an essential cofactor for mitochondrial complex I activity in the electron transport chain (3), we sought to determine whether pyrimidine depletion inhibited complex I activity. Pyrimidine depletion caused by DHODH inhibition in wild-type (WT) cells or uridine withdrawal in Δ UMPS cells caused a significant decrease in mitochondrial complex I activity in live HEK293E cells, which was recovered by UMPS cDNA expression (Fig. 2, K and L). Thus, pyruvate oxidation, PDH activity, mitochondrial NADH maintenance, and complex I activity all appear to require cellular pyrimidines.

Maintenance of thiamine pyrophosphate synthesis in cells by pyrimidine nucleotides

To determine how pyrimidine depletion affects PDH activity, we examined PDH phosphorylation by pyruvate dehydrogenase kinases (PDKs), which reduces PDH activity (23, 24). However, pyrimidines appeared to regulate PDH independently of PDK (fig. S6A). We explored the impact of pyrimidine depletion on CoA availability because CTP functions in CoA synthesis (25, 26), but pyrimidine depletion did not affect abundance of CoA (fig. S6B). Moreover, pyrimidine depletion did not affect amounts of newly synthesized CoA (M+4), as determined by stable isotope tracing with [¹³C₃-¹⁵N]-pantothenate (M+4) (fig. S6, C and D).

We conducted untargeted metabolite profiling in Δ CAD HeLa cells grown with or without uridine for 4 or 16 hours (Fig. 3A and tables S3 and S4). Changes in pyrimidine abundance enriched the abundance of specific metabolites

from various metabolic pathways, including pyruvate, thiamine (vitamin B1), methionine, tyrosine, and glucose metabolism (Fig. 3B). Thiamine is a metabolite precursor required to maintain pyruvate oxidation (27, 28). Thiamine is phosphorylated by thiamine pyrophosphate kinase 1 (TPK1) to produce thiamine pyrophosphate (TPP) (29), which functions in pyruvate decarboxylation through PDH E1 activity (30). TPP is also required for transketolase (TKT), oxoglutarate dehydrogenase (OGDH), and branched-chain alpha-keto acid dehydrogenase (BCKDH) reactions (31) (Fig. 3C). Chemical or genetic inhibition of pyrimidine synthesis significantly decreased amounts of TPP in HeLa, HEK293E, and mES cells (Fig. 3, D to F, and fig. S6E). Genetic depletion of TPK1 decreased abundance of TPP, pyruvate catabolism, and amounts of the product of TKT sedoheptulose 7-phosphate (fig. S6, F to I). Thus, it appeared that TPK1 activity might be regulated by pyrimidine concentrations. To test this, we monitored cellular TPP synthesis through stable isotope tracing using [¹³C₄]-thiamine labeling (Fig. 3G). Depletion of uridine in Δ UMPS cells decreased amounts of TPP (M+4) (Fig. 3H and fig. S6J) without affecting TPK1 protein abundance (fig. S6K). Additionally, BRQ suppressed TPP synthesis, but MTX did not (Fig. 3I), indicating that uridine or cytidine nucleotides govern TPP synthesis. Mice treated with BRQ or PRZ also showed decreased abundance of TPP in liver and a decrease in UTP without any change in abundance of ATP (Fig. 3J), indicating that cellular pyrimidines have a specific role in mouse-liver TPP synthesis.

To assess the contribution of ATP to TPP synthesis, we compared TPK1 activity in Δ UMPS and Δ GART cells cultured in the presence or absence of uridine or inosine, respectively. Inosine depletion reduced cellular abundance of ATP but not TPP synthesis in Δ GART cells (Fig. 3K), whereas uridine deprivation decreased abundance of TPP (M+4) in Δ UMPS cells. These findings indicated that pyrimidines, not purines, limit cellular TPP synthesis (Fig. 3L).

Pyrimidine depletion also affected the activity of other TPP-utilizing enzymes, such as TKT, OGDH, and BCKDH, as detected by metabolic reaction-specific isotope tracing methods. TKT activity was attenuated by pyrimidine depletion, as reflected by the decrease in sedoheptulose 7-phosphate (M+7) derived from glucose (M+6) (fig. S7, A and B). Depletion of pyrimidines also reduced OGDH activity, reflected by the decrease in succinyl-CoA (M+2) from the [¹³C₂]-acetate tracer, which incorporates into succinyl-CoA independently of acetyl-CoA derived from PDH activity (fig. S7, C and D). Pyrimidine depletion similarly decreased BCKDH activity as monitored by ¹³C₂-leucine isotope tracing into acetyl-CoA (M+1) (fig. S7, E and F). Given that PDH has a low affinity for TPP compared with that of TKT or OGDH (32, 33), PDH activity is likely

more sensitive to acute TPP depletion than are other TPP-dependent enzymes. These findings demonstrate that pyrimidines can support cellular TPP production and central carbon metabolism.

Requirement of uridine triphosphate for TPK1 activity and pyruvate catabolism

Textbooks have stated that TPK1 uses ATP to phosphorylate thiamine and produce TPP (34, 35). However, TPK1 might also use pyrimidine nucleotides directly instead of ATP to promote thiamine phosphorylation and TPP synthesis. *In vitro* enzymatic studies showed that TPK1 can use various nucleotides as phosphodonor, including UTP, without any clear specificity (36, 37). We therefore explored whether TPK1 uses UTP in human cells and sustains pyruvate oxidation.

We tested whether exogenous nucleotides could replenish abundance of TPP in digitonin-permeabilized cells that had been depleted of pyrimidines (38) (Fig. 4A). The addition of UTP, but not CTP, ATP, or GTP, effectively restored cellular TPP levels and promoted pyruvate catabolism (Fig. 4, B and C, and fig. S8, A to D). Additionally, exogenous UTP restored TCA-cycle metabolism in pyrimidine-depleted cells (Fig. 4D), indicating that UTP is required for TPP synthesis and pyruvate oxidation. A decline in pyruvate oxidation occurred when cellular UTP concentrations dropped by ~50% (fig. S8E). Moreover, direct addition of TPP to permeabilized Δ UMPS cells partially restored pyruvate catabolism, indicating that TPP depletion resulting from depletion of cellular pyrimidines can contribute to regulation of pyruvate oxidation (Fig. 4E and fig. S8F). Moreover, the depletion of CTP in cells genetically depleted of CTPS1 and 2 did not affect pyruvate catabolism, further supporting the notion that UTP, but not CTP, supports pyruvate catabolism in human cells (fig. S8G).

To determine the phosphodonor preference of TPK1 for thiamine phosphorylation, we incubated purified human TPK1 with thiamine, UTP, ATP, or CTP. Although TPK1 catalyzed TPP synthesis from UTP, ATP, or CTP, UTP was the preferred substrate for TPK1 in producing TPP (fig. S9, A to C). TPK1 showed a ~10-fold higher affinity for UTP than ATP (K_m _{UTP} = 0.33 mM; K_m _{ATP} = 5 mM) and displayed higher catalytic efficiency (k_{cat}/K_m) when incubated with UTP instead of ATP (Fig. 4F and fig. S9D) (k_{cat} , catalytic rate constant; K_m , Michaelis constant). We conducted an equilibrium binding assay with radioactive UTP and purified human TPK1, in which unlabeled UTP completely displaced the bound radiolabeled UTP from human TPK1 (Fig. 4G), demonstrating specific and direct binding. Through virtual screening for nucleotide binding sites on the TPK1 structure, we identified highly conserved residues within two helices that potentially

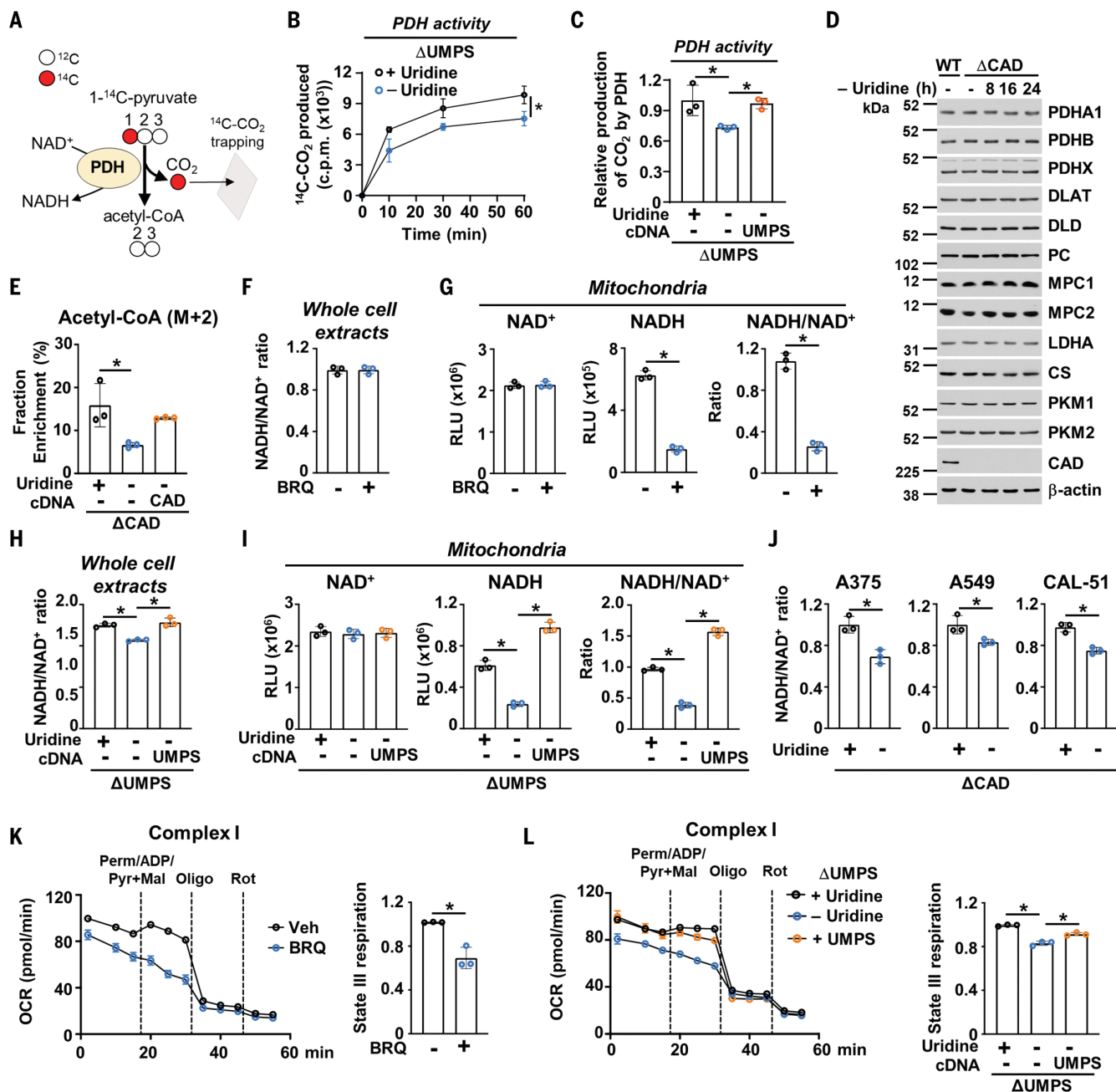


Fig. 2. Pyrimidines are required to support PDH and mitochondrial complex I activities. (A) Schematic illustrating the decarboxylation of pyruvate step mediated by PDH. (B) and (C) ¹⁴CO₂ production from [1-¹⁴C]-pyruvate, reflecting PDH activity in Δ UMPS HEK293E cells cultured in the presence or absence of uridine (200 μ M) (B), reconstituted or not with a UMPS cDNA construct (C). (D) Immunoblots of wild-type (WT) and Δ CAD HEK293E cells cultured in the presence or absence of uridine (200 μ M) for the indicated times. (E) Normalized peak areas of ¹³C-labeled acetyl-CoA derived from [¹³C₃]-pyruvate labeling in Δ CAD HEK293E cells reconstituted or not with CAD cDNA, cultured in the presence or absence of uridine (200 μ M, 16 hours). (F) Measurement of NADH/NAD⁺ ratio from whole-cell extracts of HeLa cells treated with vehicle (DMSO) or BRQ (1 μ M, 16 hours). (G) NAD⁺, NADH levels, and ratio measured from isolated mitochondria of HeLa cells treated with vehicle (DMSO) or BRQ (1 μ M, 16 hours). (H) and (I) Same as

shown in (F) and (G) but in Δ UMPS HEK293E cells reconstituted or not with UMPS cDNA, in the presence or absence of uridine (200 μ M, 16 hours). (J) NADH/NAD⁺ ratios of isolated mitochondria from A375, A549, and CAL-51 cells deleted for CAD (Δ CAD), in the presence or absence of uridine (200 μ M, 16 hours). (K) Measurement of respiratory complex I activity and quantification of state III respiration in HeLa WT cells treated with vehicle (DMSO) or BRQ (1 μ M, 16 hours). (L) Same as shown in (K) but in Δ UMPS HEK293E cells reconstituted or not with UMPS cDNA, in the presence or absence of uridine (200 μ M, 16 hours). Graphs representative of three replicates shown in (K) and (L). For all other panels, data are mean \pm SD, $n = 3$ independent replicates. * $P < 0.05$ for multiple comparisons calculated using one-way ANOVA with Tukey's HSD test [(C), (E), (H), (I), and (L)] or using a two-tailed Student's *t* test for pairwise comparisons [(B), (F), (G), (J), and (K)].

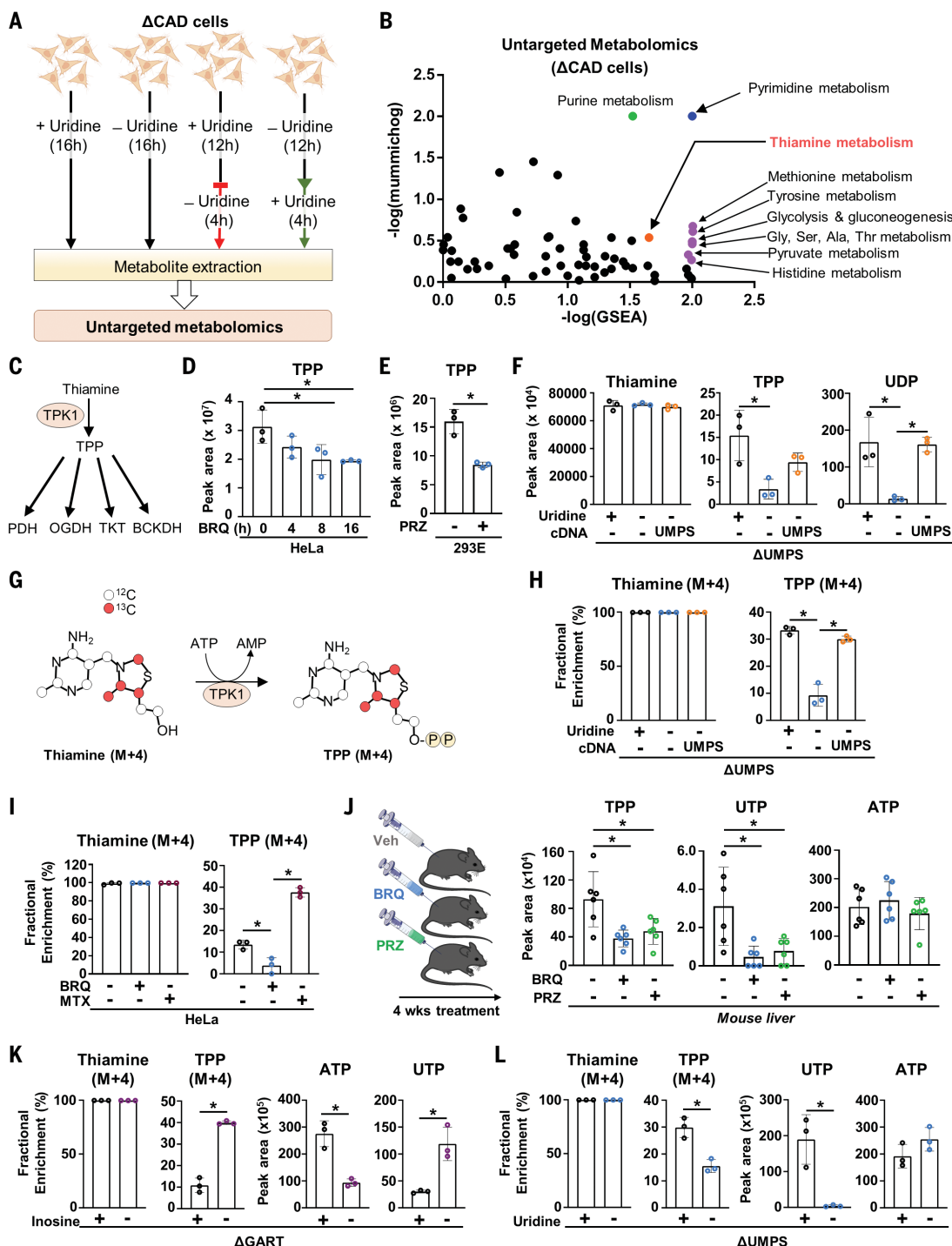
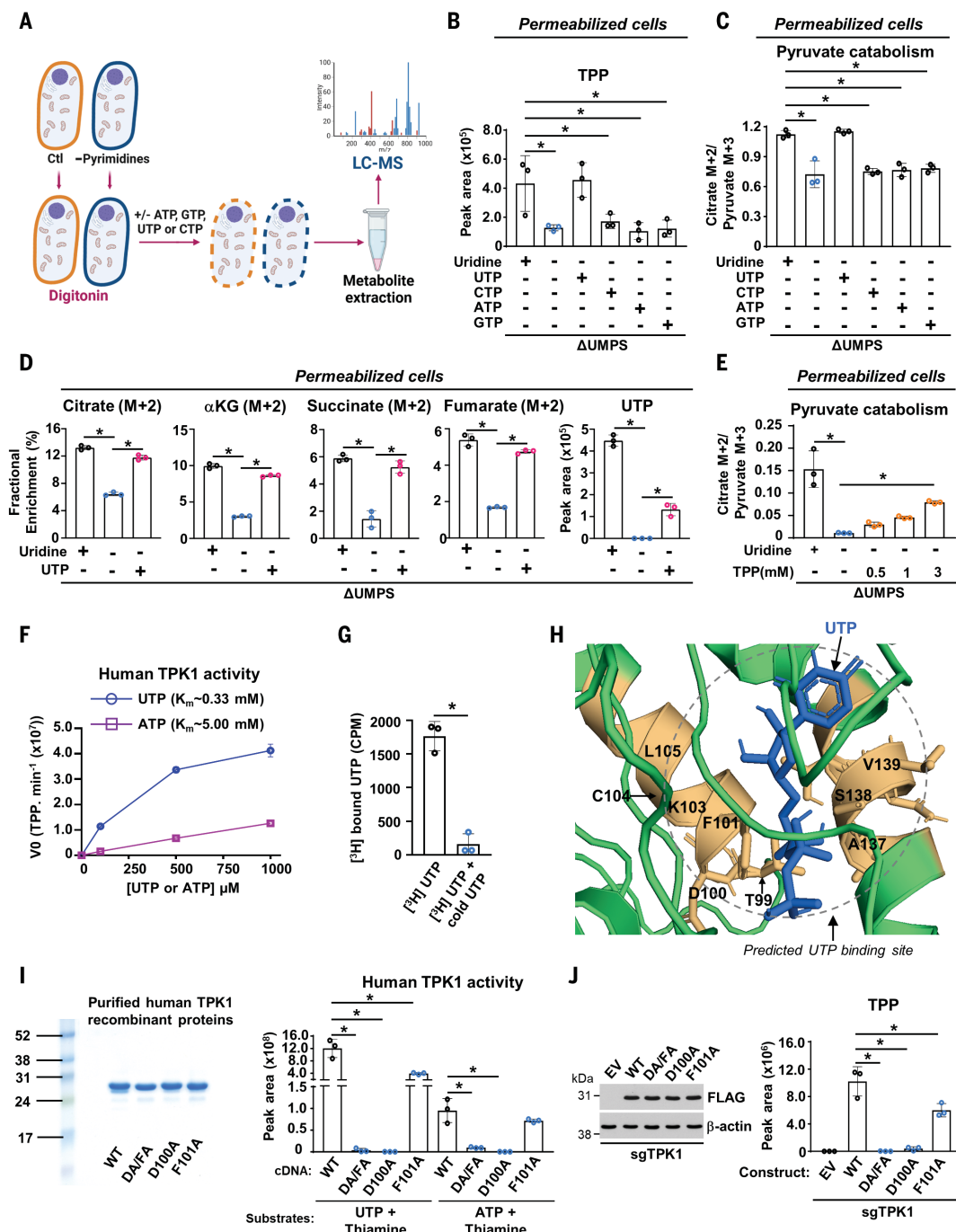


Fig. 3. Cellular pyrimidine levels are required for thiamine pyrophosphate synthesis. (A) Experimental design of the untargeted metabolomics experiment in Δ CAD HEK293E cells. (B) Pathway impact analysis of untargeted metabolomics. (C) Metabolic role of thiamine in cells. (D and E) Steady-state levels of thiamine pyrophosphate (TPP) measured by LC-MS in HeLa (D) and HEK293E (E) cells treated with vehicle (DMSO), BRQ (1 μ M), or PRZ (1 μ M). (F) Steady-state levels of thiamine, TPP, and UDP in Δ UMPS HeLa cells reconstituted or not with UMPS cDNA, in the presence or absence of uridine (200 μ M, 16 hours). (G) Cellular TPP kinase 1 (TPK1) activity measured with stable isotope tracing through measurement of carbon flow from $^{13}\text{C}_4$ -thiamine into TPP. (H) Fractional enrichment (%) of ^{13}C -labeled metabolites derived from $^{13}\text{C}_4$ -thiamine in Δ UMPS HeLa cells reconstituted or not with UMPS cDNA in the presence or absence of uridine (200 μ M, 16 hours). (I) Fractional

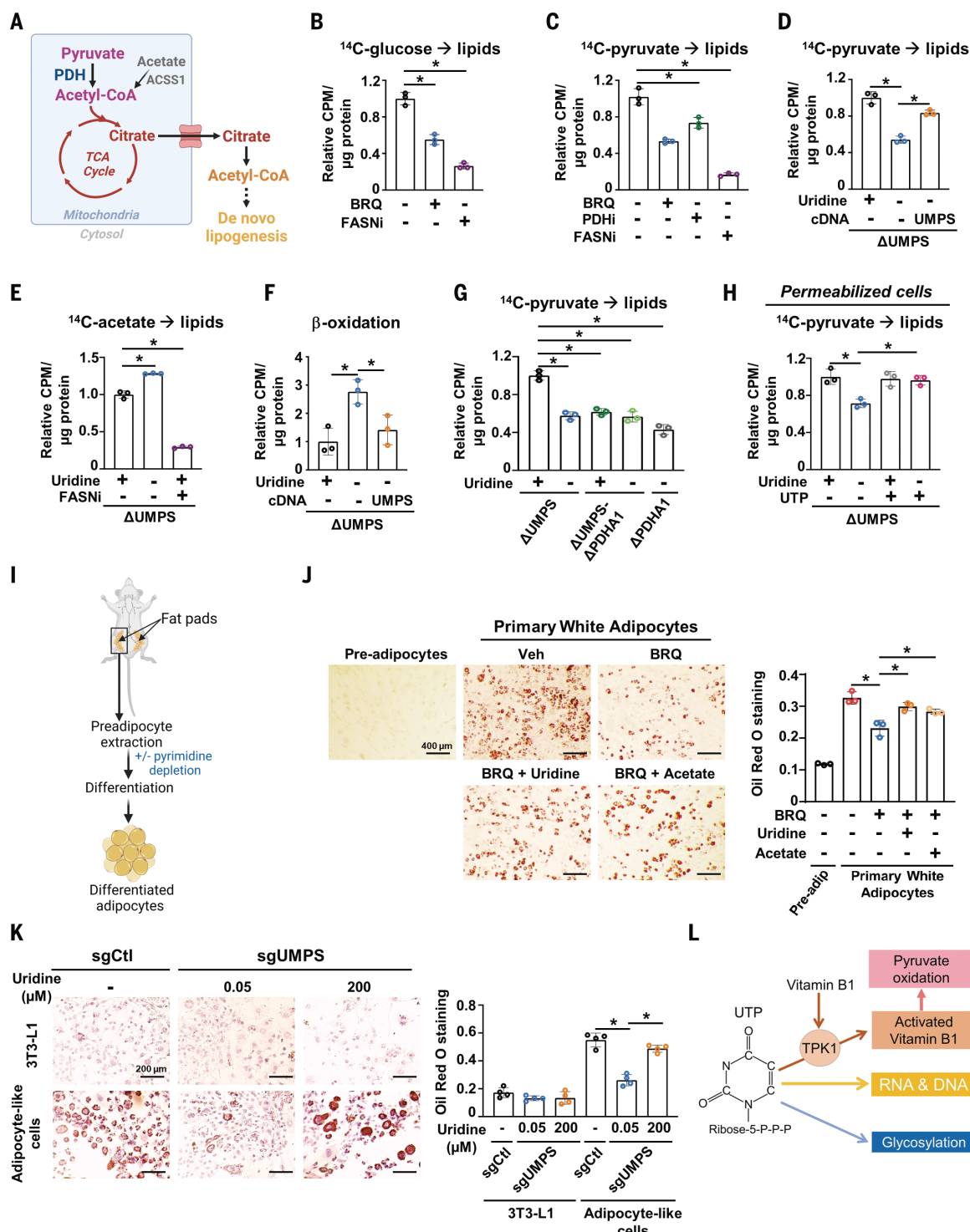
enrichment (%) of ^{13}C -labeled metabolites derived from $^{13}\text{C}_4$ -thiamine in HeLa cells treated with vehicle (DMSO), BRQ (1 μ M), or methotrexate (MTX, 4 μ M) for 16 hours. (J) Experimental design and steady-state levels of TPP, UTP, and ATP from the liver of mice treated with either vehicle (PEG-400 30%, PBS 70%), BRQ (20 mg/kg), or PRZ (10 mg/kg) over 30 days. (K and L) Fractional enrichment (%) of ^{13}C -labeled metabolites derived from $^{13}\text{C}_4$ -thiamine in Δ GART or Δ UMPS HeLa cells, cultured in the presence or absence of uridine or inosine (200 μ M, 6 hours). Normalized peak areas of ATP and UTP are shown. Data in (J) are mean \pm SD. $n = 6$ mice. For all the other panels, data are mean \pm SD. $n = 3$ independent replicates. * $P < 0.05$ for multiple comparisons calculated using one-way ANOVA with Tukey's HSD test [(D), (F), (H), (I), and (J)] or by a two-tailed Student's *t* test for pairwise comparisons [(E), (K), and (L)].

**Fig. 4. UTP is a substrate of TPK1 and supports pyruvate oxidation.**

(A) Workflow of cellular permeabilization coupled with LC-MS/MS. (B) Steady-state levels of TPP from Δ Umps HEK293E cells cultured in the presence or absence of uridine (200 μ M), digitonin (10 μ M), and supplemented with either vehicle (water) or the indicated nucleotides (200 μ M) for 8 hours prior to metabolite extraction.

(C) Citrate (M+2)/pyruvate (M+3) enrichment ratio from Δ Umps HEK293E cells treated as in (B) but labeled with [$^{13}\text{C}_3$]-pyruvate for 3 hours. (D) Fractional enrichment (%) of ^{13}C -labeled metabolites derived from [$^{13}\text{C}_3$]-pyruvate labeling in Δ Umps HEK293E cells measured and treated as in (C). Normalized peak areas of UTP are shown. (E) Citrate (M+2)/pyruvate (M+3) ratio from Δ Umps HEK293E cells treated as in (B) and (C) but supplemented with indicated concentration of TPP and labeled with [$^{13}\text{C}_6$]-glucose for the final 4 hours. (F) Kinetic assays with human TPK1 purified from *E. coli* incubated with increasing concentrations of UTP or ATP over time. The product TPP was detected by LC-MS/MS. (G) Binding of radiolabeled UTP to TPK1.

Cold UTP was added where indicated. (H) Virtual ligand screening and docking simulation for UTP on human TPK1 identified putative UTP binding pocket. (I) SDS-polyacrylamide gel electrophoresis (PAGE), followed by Coomassie blue staining, was used to analyze human TPK1 protein preparation from *E. coli*. TPP levels measured by LC-MS from purified human WT or mutants TPK1 incubated with thiamine (1 mM), UTP (1 mM), or ATP (1 mM). (J) Immunoblots and TPP levels from sgTPK1 HEK293E cells reconstituted with empty vector (EV), WT, D100A/F101A (DA/FA), D100A, or F101A human TPK1. * $P < 0.05$ calculated using a one-way ANOVA with Tukey's HSD test for multiple comparisons [(B) to (E), (I), and (J)] or a two-tailed Student's *t* test for pairwise comparisons (G). Single-letter abbreviations for the amino acid residues are as follows: A, Ala; C, Cys; D, Asp; F, Phe; K, Lys; L, Leu; S, Ser; T, Thr; V, Val. In the mutants, other amino acids were substituted at certain locations; for example, D100A indicates that aspartic acid at position 100 was replaced with alanine.

**Fig. 5. Maintenance of de novo lipogenesis and adipocyte differentiation**

by UTP. (A) Schematic illustrating the central role of citrate downstream of PDH for the maintenance of de novo lipogenesis. (B) Relative incorporation of ^{14}C from [U^{14}C]-glucose into lipids in HEK293E cells treated with vehicle (DMSO), BRQ (1 μM , 16 hours), or GSK 2194069 (FASNi, 20 μM , 16 hours). (C) ^{14}C incorporation from [2^{14}C]-pyruvate into lipids in 3T3-L1 fibroblasts treated with vehicle (DMSO), BRQ (1 μM , 16 hours), CPI-613 (PDHi, 100 μM , 16 hours), or GSK 2194069 (FASNi, 20 μM , 16 hours). (D) ^{14}C incorporation from [2^{14}C]-pyruvate into lipids in ΔUMPS HEK293E cells cultured in the presence or absence of uridine (200 μM , 16 hours), stably reconstituted or not with UMPS cDNA.

(E) ^{14}C incorporation from [1^{14}C]-acetate into lipids in ΔUMPS HEK293E cells cultured and treated as in (D). For a positive control, cells were treated with GSK 2194069 (FASNi, 20 μM , 3 hours). (F) ΔUMPS HEK293E cells reconstituted or not with UMPS cDNA, in the presence or absence of uridine (200 μM , 16 hours) and labeled with radioactive [1^{14}C]-palmitate. Measurement of ^{14}C -carbon dioxide reflects fatty acid oxidation. (G) ^{14}C incorporation from [2^{14}C]-pyruvate into lipids in ΔUMPS , ΔPDHA1 , or $\Delta\text{UMPS}/\Delta\text{PDHA1}$ HEK293E cells treated as in (D). (H) ^{14}C incorporation from [2^{14}C]-pyruvate into lipids in ΔUMPS HEK293E cells cultured in the presence or absence of uridine (200 μM), permeabilized with digitonin (10 μM), and treated with vehicle (water) or UTP (1 mM) for 8 hours and labeled with

[2^{14}C]-pyruvate for the last 2 hours. (J) Schematic illustrating the adipocyte differentiation of primary preadipocytes extracted from mouse fat pads. (K) Adipocyte differentiation of mouse primary white preadipocytes treated with vehicle (DMSO) or BRQ (200 nM) for 4 days in the presence or absence of uridine (200 μM) or acetate (1 mM). Oil red O staining and quantification are shown. (L) Adipocyte differentiation of sgUMPS

3T3-L1 fibroblasts cultured in the presence of high (200 μM) or low (50 nM) concentration of uridine. Oil red O staining and quantification are shown. (L) Regulation of vitamin B1 metabolism and pyruvate oxidation by UTP levels. Data are mean \pm SD. $n = 3$ independent replicates. * $P < 0.05$ for multiple comparisons calculated using a one-way ANOVA with Tukey's HSD test [(B) to (H), and (K)].

form a UTP-binding pocket (Fig. 4H and fig. S9, E and F). We used site-directed mutagenesis of these conserved residues of TPK1 to generate various TPK1 mutants (fig. S9G). The double mutants D100A and F101A had reduced TPK1 activity when incubated with UTP or ATP (Fig. 4I and fig. S9H) and showed diminished UTP or ATP binding to TPK1 (fig. S9I). The D100 residue was required for both UTP- and ATP-mediated catalysis (Fig. 4I), whereas the F101A single mutation impaired only TPK1's capacity to synthesize TPP from UTP (Fig. 4I). To test whether the UTP-binding sites of TPK1 promote cellular TPP synthesis and pyruvate catabolism, we established cells lacking TPK1 (*sgTPK1*) (fig. S10A) and reconstituted them with empty vector or with vectors encoding WT TPK1 or mutant variants of TPK1 (D100A and F101A) (Fig. 4J). Expression of WT TPK1 in *sgTPK1* cells restored TPP synthesis, whereas cells expressing D100A or F101A TPK1 made smaller amounts of TPP (Fig. 4J). Moreover, cells expressing D100A TPK1 displayed decreased pyruvate catabolism compared with that of *sgTPK1* cells reconstituted with WT TPK1 (fig. S10, B to D). These findings reveal a specific role for UTP in controlling TPP synthesis and pyruvate catabolism in human cells.

Pyrimidines control de novo lipogenesis and adipocyte differentiation

Our work indicates that UTP concentrations influence TPP synthesis and citrate synthesis downstream of PDH. Citrate can exit mitochondria and contribute to the production of fatty acids in the cytosol as acetyl-CoA, in addition to being used by the TCA cycle (Fig. 5A). To evaluate the effects of pyrimidine depletion on de novo lipogenesis, we quantified the incorporation of carbons from [^{14}C]-glucose, [^{14}C]-pyruvate, or [^{14}C]-acetate into lipids in HEK293E, HeLa cells, and mouse fibroblasts. As a control, we treated cells with a selective fatty acid synthase inhibitor (FASNi, GSK 2194069) or a PDH inhibitor (PDHi, CPI-613). FASNi significantly reduced lipogenesis (Fig. 5, B and C, and fig. S11A). Pyrimidine depletion with BRQ in HEK293E cells or mouse 3T3-L1 fibroblasts diminished de novo lipogenesis compared with that of control cells (Fig. 5, B and C, and fig. S11A). These effects were similar to those in cells either expressing TPK1 D100A or inhibited for PDH and TPK1 (Fig. 5C and fig. S11, B to D). Pyrimidine depletion decreased pyruvate catabolism and TPP concentrations in 3T3-L1 fibroblasts (fig. S11E). Moreover, uri-

dine depletion in ΔUMPS cells also decreased de novo lipogenesis in cells labeled with [2^{14}C]-pyruvate (Fig. 5D) but not in cells labeled with [1^{14}C]-acetate (Fig. 5E), indicating that pyrimidine regulation of lipogenesis may occur through control of PDH. Consistent with a decrease in fatty acid synthesis, measurement of the fatty acid β -oxidation through [1^{14}C]-palmitate labeling revealed that ΔUMPS cells depleted of uridine had increased mitochondrial β -oxidation (Fig. 5F).

To confirm the role of PDH in the effects of pyrimidine concentrations on lipogenesis, we generated HEK293E cells lacking *PDHA1* as well as *UMPS* and *PDHA1* (ΔPDHA1 - ΔUMPS) through modification with CRISPR-Cas9 (fig. S11F). Loss of *PDHA1* and depletion of uridine in ΔUMPS cells decreased lipogenesis (Fig. 5G), and depletion of uridine in ΔUMPS - ΔPDHA1 cells did not further decrease pyruvate-dependent lipogenesis, suggesting that pyrimidine concentrations predominantly influence lipogenesis by regulating PDH (Fig. 5G). Because UTP is necessary for TPP synthesis and pyruvate oxidation, we tested whether supplementing permeabilized cells with UTP could prevent pyrimidine depletion from inhibiting lipogenesis. UTP supplementation effectively restored lipogenesis in ΔUMPS and *ACAD* cells depleted of uridine (Fig. 5H and fig. S11G). Given the modulation of lipogenesis in response to changes in intracellular pyrimidine concentrations, we tested further whether pyrimidines might influence adipogenesis. We examined the ability of mouse primary preadipocytes to undergo white-adipocyte differentiation in the presence or absence of a low dose of BRQ (Fig. 5I). Low-dose BRQ reduced adipogenesis of primary adipocytes (Fig. 5J). Similarly, DHODH inhibition decreased adipogenesis of 3T3-L1 fibroblasts without any discernible impact on their mitotic clonal expansion capability (fig. S11, H to K). Exogenous uridine or acetate partially rescued the antidiifferentiation effects induced by pyrimidine depletion (Fig. 5J and fig. S11I). Furthermore, 3T3-L1 fibroblasts lacking *Umps* (*sgUmps*) (fig. S12A) also exhibited decreased adipocyte differentiation capacity when cultured with a low concentration of uridine (50 nM), and this phenotype was rescued by increasing uridine concentration in the medium or by supplementation with acetate (Fig. 5K and fig. S12B). 3T3-L1 cells deficient in TPK1 (*sgTpki*) or PDH (*sgPdh1*) also displayed decreased adipocyte differentiation (fig. S12, C and D). Overall, we demonstrated that the pyrimidine nucleotide UTP supports cellular TPP

synthesis and mitochondrial pyruvate oxidation, enabling citrate utilization for de novo lipogenesis and adipocyte differentiation (Fig. 5L and fig. S13).

Discussion

Control of pyruvate oxidation has been primarily attributed to PDK-dependent phosphorylation of PDH (27, 39). However, our study reveals a role of pyrimidines in regulating pyruvate catabolism across different species. We found that pyrimidines, not purines, stimulated pyruvate catabolism by controlling TPK1 activity, which promotes TPP synthesis, an essential cofactor for PDH. We discovered that TPK1 effectively utilizes UTP, rather than ATP, for cellular TPP generation. Purines, on the other hand, do not limit TPP synthesis or pyruvate catabolism. As a result, UTP emerges as a potentially important phosphodonor for vitamin B1 metabolism. Thiamine utilization has been linked to cancer cell growth and treatment, underscoring the importance of understanding its regulation in human cells (40, 41). The pyrimidine-dependent control of TPP availability and PDH activity drives the fate of intermediates downstream of pyruvate, such as citrate, which can either be catabolized into the TCA cycle, recycled into the TCA cycle, or directly used for lipid synthesis (42, 43). Although UTP is required for pyruvate oxidation and TPP synthesis, the decrease in amounts of TPP in cells depleted of UTP is partially responsible for the inhibition of pyruvate oxidation. Thus, additional UTP-dependent mechanisms that contribute to PDH regulation might exist. Depletion of cellular pyrimidines led to decreases in both PDH activities and TCA-cycle activities, which, in turn, resulted in decreased mitochondrial NADH generation and impaired complex I activity and respiration. This finding unveils the possible role of pyrimidines in controlling adipocyte differentiation through the regulation of lipogenesis. We conclude that changes in UTP concentrations may have previously unrecognized influences on thiamine utilization, pyruvate catabolism, and cell fate.

REFERENCES AND NOTES

1. A. N. Lane, T. W. Fan, *Nucleic Acids Res.* **43**, 2466–2485 (2015).
2. J. Zhu, C. B. Thompson, *Nat. Rev. Mol. Cell Biol.* **20**, 436–450 (2019).
3. I. Martínez-Reyes, N. S. Chandel, *Nat. Commun.* **11**, 102 (2020).
4. M. G. Vander Heiden et al., *Cold Spring Harb. Symp. Quant. Biol.* **76**, 325–334 (2011).
5. E. Villa, E. S. Ali, U. Sahu, I. Ben-Sahra, *Cancers* **11**, 688 (2019).
6. G. Li, D. Li, T. Wang, S. He, *Int. J. Mol. Sci.* **22**, 10253 (2021).
7. F. Del Caño-Ochoa, M. Moreno-Morcillo, S. Ramón-Maiques, *Subcell. Biochem.* **93**, 505–538 (2019).

8. V. Aleman, P. Handler, *J. Biol. Chem.* **242**, 4087–4096 (1967).
9. K. Shostak, M. E. Jones, *Biochemistry* **31**, 12155–12161 (1992).
10. M. E. Jones, *Annu. Rev. Biochem.* **49**, 253–279 (1980).
11. M. Goto, R. Omi, N. Nakagawa, I. Miyahara, K. Hirotsu, *Structure* **12**, 1413–1423 (2004).
12. H. L. Schultheisz, B. R. Szymczyna, L. G. Scott, J. R. Williamson, *J. Am. Chem. Soc.* **133**, 297–304 (2011).
13. T. Mio, T. Yabe, M. Arisawa, H. Yamada-Okabe, *J. Biol. Chem.* **273**, 14392–14397 (1998).
14. A. L. Wolfe *et al.*, *Proc. Natl. Acad. Sci. U.S.A.* **118**, e2103592118 (2021).
15. E. P. Kennedy, S. B. Weiss, *J. Biol. Chem.* **222**, 193–214 (1956).
16. D. B. Ostrander, D. J. O'Brien, J. A. Gorman, G. M. Carman, *J. Biol. Chem.* **273**, 18992–19001 (1998).
17. G. Weber, M. A. Lea, H. J. Hird Convery, N. B. Stamm, *Adv. Enzyme Regul.* **5**, 257–298 (1967).
18. A. I. Jonckheere, J. A. Smeitink, R. J. Rodenburg, *J. Inherit. Metab. Dis.* **35**, 211–225 (2012).
19. M. Bajzikova *et al.*, *Cell Metab.* **29**, 399–416.e10 (2019).
20. M. H. Soflaee *et al.*, *Nat. Commun.* **13**, 2698 (2022).
21. R. A. Saxton, D. M. Sabatini, *Cell* **168**, 960–976 (2017).
22. A. J. Valvezan, B. D. Manning, *Nat. Metab.* **1**, 321–333 (2019).
23. M. J. Holness, M. C. Sudgen, *Biochem. Soc. Trans.* **31**, 1143–1151 (2003).
24. S. Zhang, M. W. Hulver, R. P. McMillan, M. A. Cline, E. R. Gilbert, *Nutr. Metab.* **11**, 10 (2014).
25. T. Kupke, *J. Biol. Chem.* **277**, 36137–36145 (2002).
26. R. Leonardi, S. Jackowski, *Ecosal Plus* **2**, 10.1128/ecosalplus.3.6.3.4 (2007).
27. L. R. Gray, S. C. Tompkins, E. B. Taylor, *Cell. Mol. Life Sci.* **71**, 2577–2604 (2014).
28. D. Lonsdale, *Evid. Based Complement. Alternat. Med.* **3**, 49–59 (2006).
29. L. de Jong, Y. Meng, J. Dent, S. Hekimi, *Genetics* **168**, 845–854 (2004).
30. J. R. Butler, R. H. Pettit, P. F. Davis, L. J. Reed, *Biochem. Biophys. Res. Commun.* **74**, 1667–1674 (1977).
31. J. A. Mayr *et al.*, *Am. J. Hum. Genet.* **89**, 806–812 (2011).
32. V. I. Bunik, A. Tylicki, N. V. Lukashev, *FEBS J.* **280**, 6412–6442 (2013).
33. J. R. Tate, P. F. Nixon, *Anal. Biochem.* **160**, 78–87 (1987).
34. M. Sambo *et al.*, *Biochim. Biophys. Acta, Gen. Subj.* **1866**, 130071 (2022).
35. L. J. Baker, J. A. Dorocke, R. A. Harris, D. E. Timm, *Structure* **9**, 539–546 (2001).
36. A. I. Voskoboyev, Y. M. Ostrovsky, *Ann. N.Y. Acad. Sci.* **378**, 161–176 (1982).
37. M. Onozuka, K. Nosaka, *J. Nutr. Sci. Vitaminol.* **49**, 156–162 (2003).
38. Y. Nonnenmacher *et al.*, *Metab. Eng.* **43**, 147–155 (2017).
39. A. R. Grassian, C. M. Metallo, J. L. Coloff, G. Stephanopoulos, J. S. Brugge, *Genes Dev.* **25**, 1716–1733 (2011).
40. J. A. Zastre, R. L. Sweet, B. S. Hanberry, S. Ye, *Cancer Metab.* **1**, 16 (2013).
41. R. Guaracujo *et al.*, *Sci. Adv.* **6**, eabc7120 (2020).
42. P. K. Arnold *et al.*, *Nature* **603**, 477–481 (2022).
43. K. E. Wellen *et al.*, *Science* **324**, 1076–1080 (2009).
44. U. Sahu *et al.*, Pyrimidines maintain mitochondrial pyruvate oxidation to support de novo lipogenesis. Dryad (2024); <https://doi.org/10.5061/dryad.rxdwbrvfq>.

ACKNOWLEDGMENTS

We thank the remaining members of the Ben-Sahra laboratory for their valuable contributions and discussions on the data presented in this manuscript. **Funding:** This work was supported by grants from the NIH (R01GM135587 and R01GM143334 to I.B.-S., 5R35CA197532 and 5P01AG049665 to N.S.C., and R35CA197569 to A.S.); the LAM Foundation Established Investigator Award (LAM0151E01-22 to I.B.-S.); and the American Cancer

Society Award (DBG-23-1039959-01-TBE to I.B.-S.). **Author contributions:** U.S. and E.V. performed all experiments and prepared the manuscript. P.G. and J.M.A. performed the LC-MS analysis. C.R.R. and N.S.C. provided expertise for metabolic experiments on animals. Z.Z. and A.S. provided the mouse embryonic stem cells. B.P.O. and M.D.T. provided technical assistance. R.M. and B.S. performed the computational analysis of the untargeted metabolomics data. I.B.-S. supervised the project, reviewed all experimental data, and prepared the manuscript. All authors discussed the results and commented on the manuscript. **Competing interests:** The authors declare that they have no competing interests. **Data and materials availability:** All constructs and cell lines established in this study are available upon request. All data are available in the main text or the supplementary materials. Raw data are archived on Dryad (44) and Mendeley Data (<https://data.mendeley.com/preview/sg634gv9v2>). **License information:** Copyright © 2024 the authors, some rights reserved; exclusive licensee American Association for the Advancement of Science. No claim to original US government works. <https://www.science.org/about/science-licenses-journal-article-reuse>

SUPPLEMENTARY MATERIALS

science.org/doi/10.1126/science.adh2771

Materials and Methods

Supplementary Text

Figs. S1 to S13

Tables S1 to S4

References (45–51)

MDAR Reproducibility Checklist

Submitted 21 February 2023; resubmitted 14 August 2023

Accepted 20 February 2024

10.1126/science.adh2771